Fluorescence properties of trendy molecules studied with synchrotron radiation

Vall-llosera, Gemma

2006

ROYAL INSTITUTE
OF TECHNOLOGY

Fluorescence properties of trendy molecules studied with synchrotron radiation

GEMMA VALL-LLOSERA

Licenciate Thesis
Stockholm, Sweden 2006

TRITA FYS 2006:57
ISSN 0280-316X
ISRN KTH/FYS/--06:57--SE
ISBN 91-7178-428-4

KTH Physics
SE-106 91 Stockholm
SWEDEN

Akademisk avhandling som med tillstånd av Kungl Tekniska högskolan framlägges till offentlig granskning för avläggande av filosofie licenciatesexamen i fysik måndagen den 9 oktober 2006 klockan 10.00 i FA31, Albanova, Kungl Tekniska högskolan, Roslagstullsbacken, 21, Stockholm.

Tryck: Universitetsservice US AB

Abstract

This thesis summarises the experimental results on molecular spectroscopy of gas phase molecules using synchrotron radiation in the UV- VUV and soft-X rays regions. The results of applying Photon Induced Fluorescence Spectroscopy (PIFS) to D_2, H_2S, H_2O and pyrimidine are presented and discussed. Both inner and outer shell excitations of free molecules lead to different relaxation processes. However, a common result is that when the molecule breaks and the resulting neutral fragments are left in an excited state, they might fluoresce in the UV- Vis range. PIFS technique has two main advantages, it permits to detect neutral fragments and to identify the fluorescing species. From this fact, we can infer dissociation channels and trace back the electronic processes that led to the fluorescence. For these molecules we have analysed and interpreted both dispersed and undispersed fluorescence. What motivates our work is the lack of fluorescence studies and in a more general sense, to contribute to the knowledge of important molecules for life such as water and pyrimidine.

Resum

Aquesta tesi és un recull dels resultats experimentals obtinguts en espectroscopia de molècules en fase gasosa utilitzant radiació sincrotró en les regions de l'UV-VUV i raigs X. La tècnica utilitzada en els nostres experiments és anomenada en anglès Photon Induced Fluorescence Spectroscopy, PIFS; es prodria traduir com: Espectroscopia de la fluorescència induïda per fotons. Doncs, els resultats d'aplicar aquesta tècnica a les molècules D_2, H_2S, H_2O i pirimidina són presentats i discutits. Excitacions a les capes internes o de València d'una molècula conduiexen a diferents processos de relaxació. No obstant i com a resultat general, quan una molècula es fragmenta i els fragments eixits són neutres i excitats, emeten fluorescència. La tècnica té dues avantages principals, ens permet de detectar fragments neutres i identificar les espècies que emeten fluorescència. D'aquí podem deduir les reaccions de fragmentació que tenen lloc i tracejar els processos electrònics que han donat lloc a la fluorescència. En l'estudi hem enregistrat i analitzat la fluorescència dispersa i no-dispersa d'aquestes molècules. La motivació principal del nostre estudi és la manca de coneixement en l'àrea i com a més general, contribuir en el coneixement de molècules importants per la vida , com l'aigua i la pirimidina.

List of papers

This thesis includes two published papers in international journals and one submitted paper being refereed.

- PAPER I *The $np\sigma, \pi$ to EF emission systems in D_2 studied by selective excitation* G. Vall-llosera, J. Álvarez Ruiz, P. Erman, E. Melero García, E. Rachlew, S. Menmuir and M. Stankiewicz *J. Phys. B: At. Mol. Opt. Phys.* **38** (2005) 659

- PAPER II *Fluorescence emission following core excitations in the water molecule* A. Kivimäki, M. Coreno, R. Richter, J. Álvarez Ruiz, E. Melero García, M. de Simone, V. Feyer, G. Vall-llosera and K. C. Prince. *J. Phys. B: At. Mol. Opt. Phys.* **39** (2006) 1101

- PAPER III *Fluorescence emission from photo-fragments after resonant S 2p excitations in H_2S* G. Vall-llosera, E. Melero García, A. Kivimäki, E. Rachlew, M. Coreno, M. de Simone, R. Richter and K.C. Prince *submitted to Physical Chemistry Chemical Physics*

Not included papers

- PAPER IV *VUV photon induced fluorescence study of SF_5CF_3* J. Álvarez Ruiz, A. Kivimäki, M. Stankiewicz, E. Melero García, M Coreno, S. Ali, J. Koperski, E. Rachlew, G. Vall-llosera, V. Feyer and R. P. Tuckett *submitted to Physical Chemistry Chemical Physics*

My contribution to the papers is as follows:

Paper I: I participated actively in the experiments. I did part of the data analysis and I am responsible for part of the writing.

Paper II: My contribution to this paper is the participation during the experimental session and in the discussions.

Paper III: I participated in the experiments. I analysed the data and I am responsible for the writing.

Acknowledgements

I am supposed to be half-way-through my PhD and the proof of it are these words you are reading now. Many people has contributed to this half-way but some of them have been essential. I would like to thank Elisabeth Rachlew, my supervisor, for many reasons. First of all, for trusting me and for being always positive with my work and having the patience to read my articles 100 times, for giving me the opportunity to do physics and for financing me! Talking about money I want to thank as well, Mats Larsson for providing me with a one year grant, really welcomed at that time, thanks! My words of gratitude also to Sheena, Mattias, Jaume, Peter Erman, Agneta Falk, Jesús and Emilio. If another person in the department has had the patience to read my articles as many times as my supervisor is Emilio (lucky you!). From him I have learned a lot (or more than that) and I got the chance to practice my spanish :-). I also want to send my gratitude to Italy where Marcello and Antti are making possible this and knitting my future. Many thanks to Marek, in England for the last-minute decisions to take part in the experiments. All the team in Max-Lab are also thanked for providing such friendly and easy-working conditions and Gas Phase Beamline staff in ELETTRA for being so professional. Outside my physics world several people are also involved. My parents, Miquel i Montserrat, for being who they are and for being proud of me. Gordana, Slavisha, Paula, Mia, Theanne, Jakob, Malin, Marianne, Elin, Anneli, Gustav, ... for making my life in Sweden easier. Back in Catalonia I want to remember Mireia, Jordi, Susanna, Núria, Roser, Toni, Mercè, Xavi, Anna, Pere, Cris, Ferran, les Cuques, the people in Òptica Muralla, Manel, marc (long life to lowercase letters) and Albert for being there and not forget me. I also want to thank Marta in Berna, Núria in Kalmar, Laia (bcn-madrid-basel, where are you?) and Ingrid in Barcelona for the annual 'floretes meetings'! (I wouldn't survive without them!). My words of gratitude to Max, for the long-lasting friendship. Finally, I would like to thank Johan (min privata sköldpadda) for being supportive and just for being here! Other people not mentioned have been a great help but I cannot mention everybody because I need to save space for the thesis itself!

Contents

List of papers **v**

Acknowledgements **vii**

Contents **viii**

Introduction **1**

I Background **3**

1 Synchrotron Radiation **5**
1.1 Types of radiation 5
1.2 How is it created? 6
1.3 Synchrotron radiation facilities 7
1.4 Max-lab 7
1.5 ELETTRA 8

2 Molecules and light **9**
2.1 What is a molecule? 9
2.2 About the interaction of molecules and light 11

3 Technique and experimental set up **13**
3.1 Photon induced fluorescence spectroscopy 13
3.2 Experimental set up 14

II Results **17**

4 Molecular deuterium, D_2 **19**

5 Water, H_2O **23**
5.1 Ly-α 23
5.2 Neutral oxygen 24

5.3 Neutral OH 25
5.4 OH^+ 26

6 Hydrogen sulphide, H_2S **29**
6.1 Total Ion Yield (TIY) and Total Fluorescence Yield (TFY) 29
6.2 Lyman and Balmer emission 30
6.3 Dispersed fluorescence 31
6.4 Branching ratios 32
6.5 Dissociation pathways 34

7 Pyrimidine, $C_4H_4N_2$ **37**

III What is next? **41**

8 Outlook **43**

Bibliography **45**

Introduction

There are many possible ways to write a thesis or as I prefer to call it, a compilation of the work I have been doing in the group of Atomic and Molecular Physics at the Physics Department at KTH (Kungliga Tekniska Högskolan) during these two years. The group is an experimental group, i.e., we explore the nature with experimental tools. During these two years I have studied the Visible-UV fluorescence emitted by synchrotron light excited molecules. I have started with some relatively small and important molecules such as D_2 and H_2O. The study is followed by H_2S which has the same hydrogen content and symmetry as water and then a jump to some small, so called, bio-molecules. So far, we have studied pyrimidine, both in inner and outer shell excitations and pyridazine in the valence region.

The technique used for our fluorescence studies is called PIFS, photon induced fluorescence spectroscopy and is the one used for the experiments in the three included papers.

So, in the following pages you can read about the samples we used and why, the set up for the fluorescence studies and the excitation source (see figure below).

I have divided the thesis in three main parts, *a background part*, a *results part* and a *future work*.

The *background* contains a description of the light source, synchrotron radiation (SR). The types of SR available, the creation of it and the synchrotron facilities we work at. Then follows a chapter where I try to define what a molecule is and describe the interaction between gas phase molecular systems and the SR. Finally, I include a section for the experimental set up and the technique used.

In the second part and as the name suggests, *Results*, the outcome of the experiments are presented. I will go through molecular deuterium first, water and

hydrogen sulphide, papers I, II and III and then I will also present the preliminary results obtained for pyrimidine, not published in any journal yet.

Finally, a third part *Overview* is added where an outlook into the future is described.

Part I

Background

Chapter 1

Synchrotron Radiation

1.1 Types of radiation

An accelerated charged particle describing a curved trajectory will emit radiation. When moving at a relativistic speed, this radiation is emitted as a narrow cone tangent to the path of the particle. Thus, synchrotron radiation is generated when relativistic electrons undergo a change of direction in a magnetic field (see Fig. 1.1). Nowadays, there are three forms of synchrotron radiation according to the three

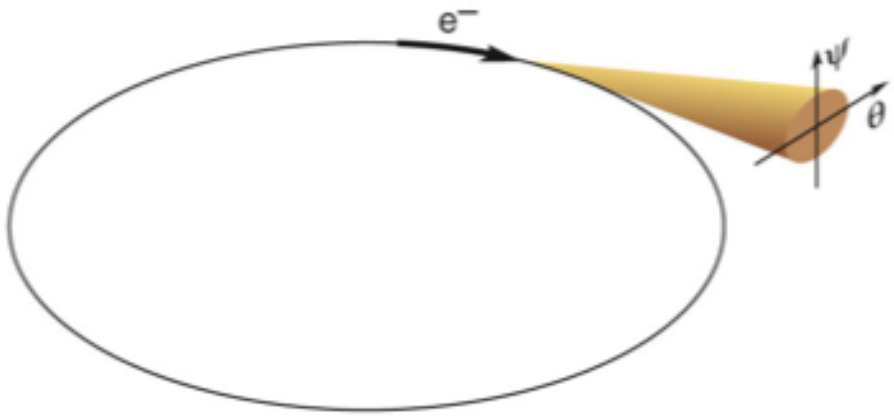

Figure 1.1: Cone of light generated by the acceleration of the electron.

types of magnetic structures used: bending magnet radiation, undulator radiation and wiggler radiation (see Fig. 1.2).

Bending magnet radiation occurs when an electron travels in a uniform magnetic field. The radiation produced is directed tangentially outwards in a narrow cone resulting in a fan of radiation around the bend, like a 'search light'. Undu-

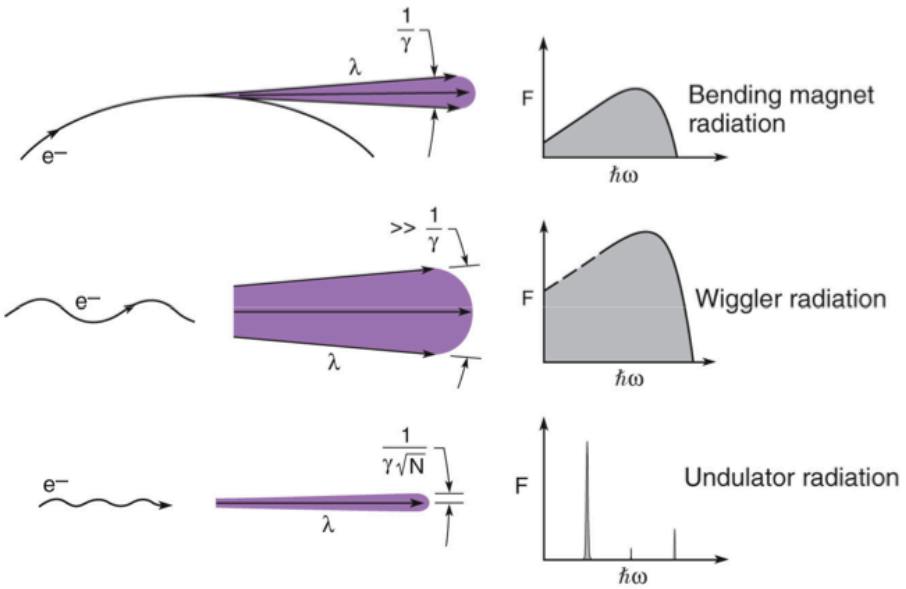

Figure 1.2: Electron trajectories, radiation cone sizes and radiation spectra for the three forms of SR. γ is the Lorentz contraction factor, λ is the wavelength and N is the number of magnetic periods. In the graphs the spectra of light are represented for the three kinds of radiation [1].

lator radiation is generated when an electron traverses a periodic, relatively weak magnetic field. The periodicity causes the electron to experience an harmonic oscillation in the axial direction (see Fig. 1.2) resulting in a motion characterized by small angular excursions called undulations. Because the magnetic field is relatively weak the amplitude of this undulation is small causing the cone to be narrow. Wiggler radiation is also generated when an electron traverses a periodic magnetic field but in this case, the magnetic field is no longer weak. Therefore, the oscillation amplitude and radiated power are larger and the radiation generated peaks at higher photon energies. The radiation spectrum is very broad, similar to that of the bending magnet.

1.2 How is it created?

An electron beam is generated in an electron gun. In order to increase the energy of this electron beam it is accelerated by electric fields e.g. in a linear accelerator (LINAC). Now the electron beam will have sufficient energy to enter the storage ring where various magnetic lenses will keep the electrons travelling along the desired trajectory. Synchrotron radiation is produced as the electrons pass through bending

magnets, undulators or wigglers.

1.3 Synchrotron radiation facilities

In our experiments we have used radiation from two synchrotron facilities. The Swedish National Synchrotron Radiation Laboratory MAX, in Lund and the ELETTRA synchrotron ring in Trieste (Italy). Below there is a description of the beamlines in each laboratory which have been used in these experiments.

1.4 Max-lab

The Max-lab facility (see Fig. 1.3) has nowadays, three rings. MAX I, MAX II and MAX III (operative by the end of 2006). Gas phase experiments in Max I have been performed in beamline 52 (BL52) and beamline I411 in Max II.

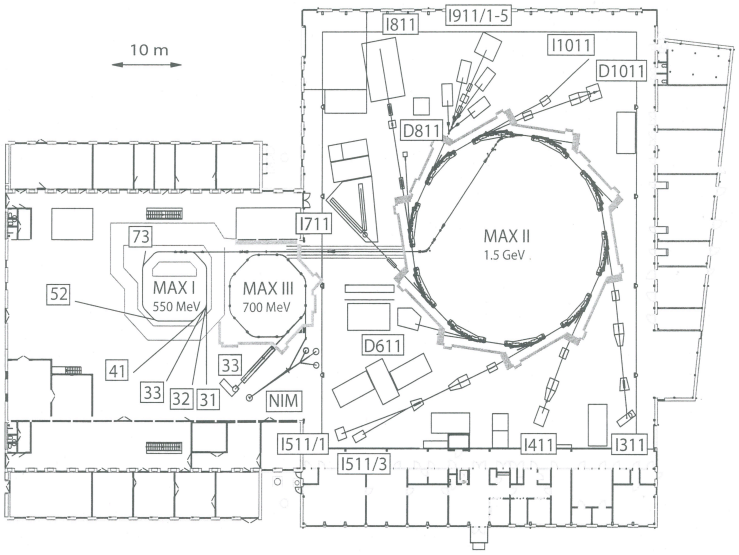

Figure 1.3: Scheme of the Max-laboratory [2].

Beamline 52

For the valence level experiments we have used radiation from a bending magnet in BL52. The radiation from the bending magnet first hits a gold coated spherical

mirror that focuses it onto the entrance slit of a 1 m normal incidence monochromator (NIM). The 1200 l/mm grating in the monochromator selects the required excitation energy in the 5-30 eV range. Then, the monochromatic radiation is focused to the exit slit, after which it enters a chamber with a toroidal refocusing mirror. There, the light is directed into the experimental chamber with a spot area at the focal point of 1-2 mm^2 [3].

Beamline I411

For core level experiments we have used the one meter section of the undulator radiation from BL I411. The beamline consists of a modified SX-700 plane grating monochromator and a plane elliptical focusing mirror set up to produce undulator radiation in the range of $50 - 1500$ eV [4].

1.5 ELETTRA

Gas phase experiments in ELETTRA are performed at The Gas Phase Photoemission Beamline. This beamline comprises an undulator source with a 125 cm period, a spherical grating monochromator equipped with a movable planar premirror and two refocusing mirrors in addition to the spherical grating (see Fig. 1.4). Altogether it provides high-intensity collimated radiation in the photon energy range 15-1500 eV and a spot size of a few hundred microns at the end of the beamline [5].

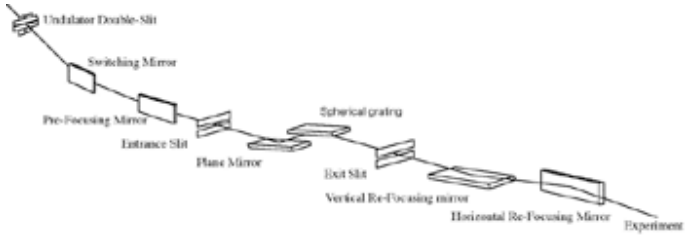

Figure 1.4: Scheme of the Gas phase beamline at ELETTRA [6].

Chapter 2

Molecules and light

2.1 What is a molecule?

A molecule, from the latin word, *molecula*, meaning "small mass", is an aggregation of atoms. The great variety of materials found in the world is the result of infinite combinations in which molecules may be constructed from the atoms in the periodic table of elements.

The simplest molecules are diatomic and homonuclear, i.e., two atoms of the same kind, such as D_2, H_2, etc. The chemical bonding, the way they share the electrons, is termed homopolar or covalent. The next simplest group is that of diatomic molecules containing two different atoms. They can bond covalently or ionically. Fig. 2.1 and Fig. 2.2 show the two types of bonds.

Figure 2.1: Example of a covalent bond with the H_2 molecule. The two electrons, one from each hydrogen, are shared and keep the atoms together. Picture taken from ref. [7].

Continuing through molecules with several atoms, such as H_2O, NH_3 we come to larger molecules such as pyrimidine ($C_4N_2H_4$) or purine ($C_5H_4N_4$) precursors of the giant[1] molecule DNA (see Fig. 2.3).

In contrast to atoms, molecules have internal degrees of freedom; their vibrational or rotational states can be excited, for example. Because of that, the band spectrum of a molecule exhibits a threefold structure: it contains a number of often clearly separated groups of bands, the so-called *band systems*; each *band system*

[1] Giant here means in the micrometer range whereas small means nanometer scale

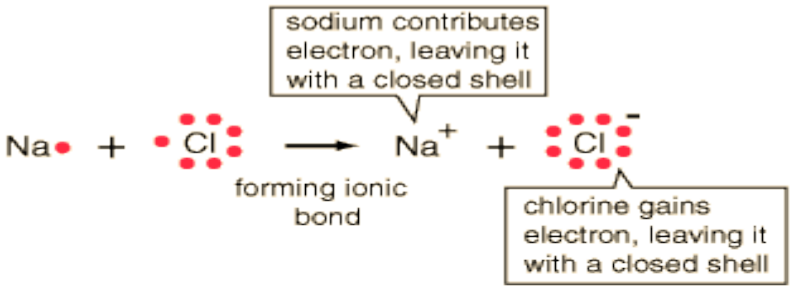

Figure 2.2: Example of an ionic bond with the $NaCl$ molecule. The electron of sodium joins the chlorine atom. The resulting positive and negative ions will attract each other. Picture taken from ref. [7].

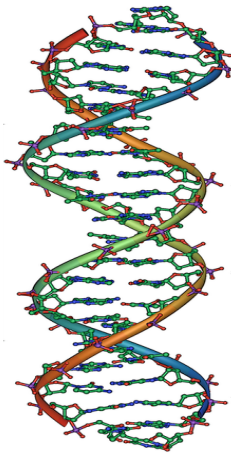

Figure 2.3: The double-helix DNA giant molecule. Picture taken from ref. [8]

consists of a number of *bands*; and each *band* is made up of a very large number of *band lines*, which occur in an ordered quantised fashion. This threefold structure of the spectrum corresponds to the three contributions to the total energy of a molecule, that is the electronic, vibrational and rotational excitations. Figure 2.4 shows the electronic, vibrational and rotational levels of a molecule in a simple way.

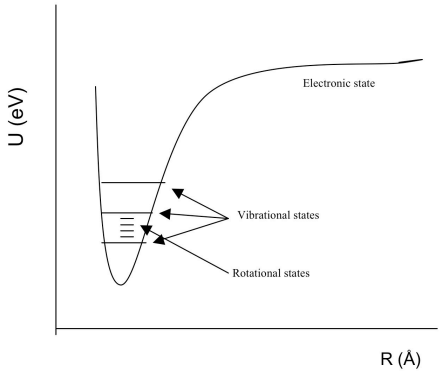

Figure 2.4: A schematic picture of a molecular electronic state as a function of interatomic distance together with the vibrational and rotational energy levels. [9]

2.2 About the interaction of molecules and light

When a molecule receives energy larger than its ionisation potential, IP, the two basic processes at the end of the chain reaction that can occur are:

1. Non-radiative emission
2. Radiative emission

Written below are some of the possible processes leading to (1) and (2).

$$AB + h\nu \rightarrow AB^* \quad \text{excitation of the molecule}$$

After excitation of one of the electrons to an empty molecular or Rydberg orbital, the excited molecule will relax mainly via autoionization or dissociation:

$AB^* \rightarrow AB^{+*} + e^-$	autoionization
$\rightarrow A^+ + B^-$	ion pair formation
$\rightarrow A + B^*$	dissociation or pre-dissociation
$\rightarrow AB(g.s.) + h\nu$	parent molecule fluorescence emission

The first process consists of removing an electron, usually from one of the outermost orbitals, so we end up with an excited molecular ion and an electron. In the second and third processes the molecule dissociates. In the fourth process the molecule relaxes to the ground state again via emission of a photon.
The excited molecular ion in process one can further dissociate:

$AB^{+*} \rightarrow A^+ + B^*$	dissociation into an ion and an excited neutral fragment
$AB^{+*} \rightarrow AB^+ + h\nu$	fluorescence emission from the excited molecular ion

Autoionisation and ion pair formation are among the processes in (1) and neutral excited fragment formation, parent molecule and molecular ion fluorescence emission will lead to the general process (2). Of all these possible processes, we study the ones leading to the general process (2), i.e., the ones that will emit fluorescence in the Vis- UV range.

Chapter 3

Technique and experimental set up

3.1 Photon induced fluorescence spectroscopy

Fluorescence studies constitute the experimental work presented in this thesis. These fluorescence studies are known under the abbreviation of PIFS which stands for photon induced fluorescence spectroscopy. Our goal is to analyse and interpret the fluorescence in the UV-visible range emitted by our sample after interacting with the synchrotron radiation.

This fluorescence can be recorded in two qualitative ways: dispersed and undispersed. In order to disperse fluorescence we need a spectrometer attached to a detector, usually a CCD detector. Because of the grating, we are able to differentiate different wavelengths and identify species fluorescing. A typical spectrum of dispersed fluorescence is shown in Fig. 3.1. For the undispersed fluorescence

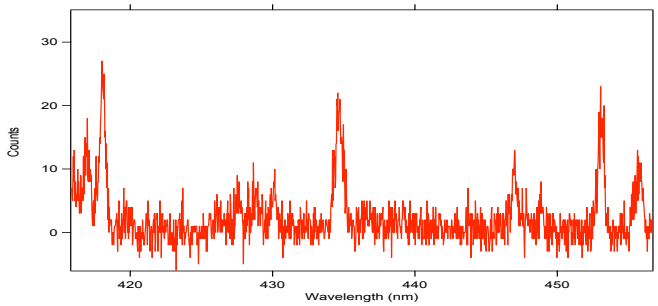

Figure 3.1: Dispersed fluorescence after core excitation of H_2S. $E_{exc} = 165.34$ eV [10]

we use photo multiplier tubes, PMTs, which gives us a digital signal proportional to the number of incident photons. In this way, we measure the total fluorescence that strikes the PMT without further discrimination. An example of undispersed

fluorescence is shown in Fig. 3.2. PIFS has been proven to be a useful technique

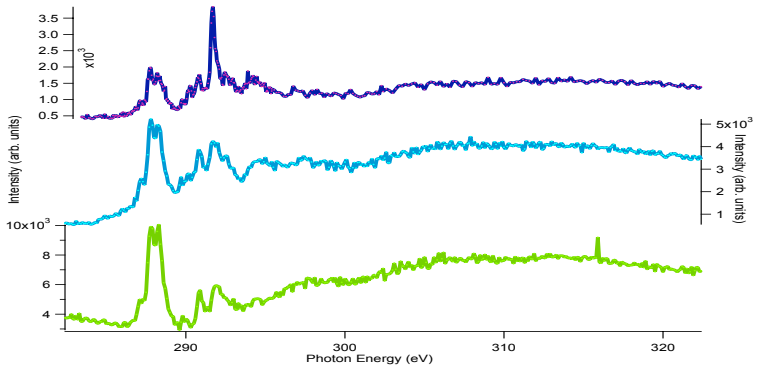

Figure 3.2: From top to the bottom; Ly-α emission, UV and visible total fluorescence yields for pyrimidine after core excitation around the C1s threshold.Vis-UV fluorescence is recorded with PMTs in the region of 300-650 nm and 115-320 nm, respectively. Ly-α signal is recorded with a PMT and a filter in front of it. The three spectra are normalised to the flux of the beamline.

for the detection of neutral fragments which could not be easily detected with other techniques e.g. photoelectron spectroscopy. Thus, we can infer the possible fragmentation paths of a system after synchrotron excitation. In our group PIFS has been used in combination with UV-VUV synchrotron radiation, i.e. for valence studies [11, 12] and more recently with soft-x ray photons, i.e. for core studies [10, 13, 14]. The articles published along with the thesis are proofs of the usefulness of the PIFS technique.

3.2 Experimental set up

Two different experimental set ups are discussed in the papers according to at which synchrotron facility the experiments are performed. Each of the papers and the references there in describe the set up. Paper I set up consists of a high-vacuum chamber (background pressure of about 10^{-6} mbar) where monochromatic synchrotron light crosses a jet of sample gas (see Fig. 3.3). Visible fluorescence light is collected by a PMT, Hamamatsu R647 (300-650 nm) detached from the vacuum region by a fused silica lens (90% transmission in the 250-1000 nm range). Dispersed fluorescence is collected perpendicular to the SR by a lens/mirror system and focused onto the entrance slit of an f = 0.46 m spectrometer (Jobin-Yvon spectrometer HR460) with a 600 gr/mm and a 1200 gr/mm grating mounted on a turret and able to cover a range of 300-900 nm. Fluorescence is recorded with a liquid nitrogen cooled CCD detector. For more extensive information on the collection

efficiency of the fluorescence system I refer the reader to [9] and for more information on the experimental chamber itself to [15]. Papers II and III set up consists

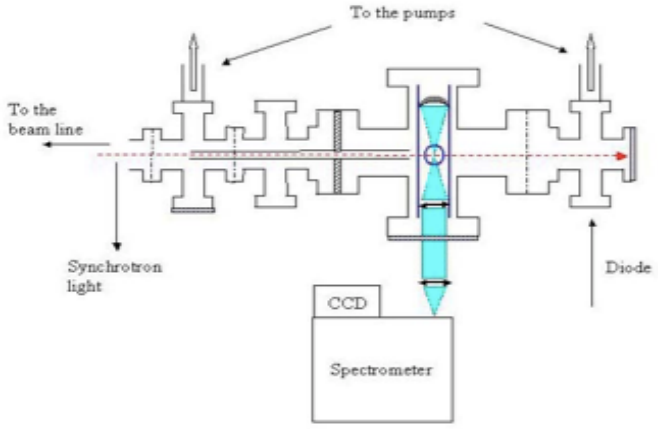

Figure 3.3: Experimental setup. The synchrotron light comes into the chamber from the left and continues to the right through a small capillary, the interaction zone and to the diode. The fluorescence coming from the interaction zone is gathered by an optical system and focused to the slit entrance of the spectrometer. Two ports of the chamber are connected to two pumps which maintain the vacuum inside [9].

of a vacuum chamber in which fluorescence is collected perpendicularly to the synchrotron beam by a spherical mirror mounted inside the chamber. The collimated light is sent through a quartz window and a lens outside the chamber focus it onto the entrance slit of a fluorescence spectrometer (Acton Spectra Pro 500) equipped with a 1200 gr/mm and a 3600 gr/mm grating mounted on a turret and able to cover a wavelength region of 250-900 nm. Dispersed photons are recorded using a liquid nitrogen cooled CCD detector (Princeton 10:100B). The entrance slit of the spectrograph can be adjusted to give total resolution of 0.1-2 nm, depending on the needs of a particular measurement. Gaseous samples are allowed into the chamber through a needle of radius ca 0.5 mm which injects the gas sample beam at the curvature center of the mirror where it meets the SR. A leak valve connected to a gas reservoir controls the pressure in the chamber. The integrated ion current can be measured with a micro-sphere plate (a 1 inch detector from El-Mul Technologies Ltd.) mounted at the entrance of the chamber perpendicularly to the direction of the beam and a diode at the back of the chamber can record the variations in the synchrotron light flux. Instead of the spectrometer we could mount different PMTs to record undispersed fluorescence in the visible or UV range. Band pass filters have been used in front of the PMTs to record the intensity from specific wavelength regions.

Part II

Results

Chapter 4

Molecular deuterium, D_2

In this article we have studied the dispersed fluorescence of molecular deuterium excited by means of synchrotron radiation. D_2, also called heavy hydrogen is a stable isotope of H. The nucleus contains a neutron and a proton (whereas H has only one proton). The potential curves for D_2 are shown in Fig. 4.1. As can be seen in the figure each of the electronic states has a quantum set of vibrational levels. The accessibility of such states depends on the selection rules, i.e., Franck-Condon factor. The figure also shows the dissociation limit for $D_2 + h\nu \rightarrow D(1s) + D(2l)$. This can be regarded as an antibonding electronic state crossing the bounding states $np\pi, np\sigma$ with $n \geq 3$.

Using monoenergetic synchrotron light in the range of $13.97 - 15.84$ eV in order to excite the D 1s electron, we reached different Rydberg states (Franck- Condon allowed states). The relaxation of the system can take place via radiative or non-radiative emission as stated in 2.2. In searching for $np\sigma, \pi - EF$ (see Fig. 4.1) fluorescence emission, it is expected that the most intense transitions terminate on the E part of the EF curve in view of the Franck- Condon principle. Actually, calculated Franck-Condon factors [16] suggest that the most intensive bands are (0;0), (1;3), (2;6) and (3;9) [1].

Thus, the detection of fluorescence will prove the radiative decay and vice-versa. Figure 4.2 shows the results for the dispersed fluorescence. The panels show one single band each except for the last one where indication of another band $4p\sigma(v = 1)$ is seen. Thus looking at Fig. 4.2 we can observe the results of exciting the molecule to high vibrational states. Figure 4.2 clearly shows the presence of pre-dissociation for the $4p\pi - EF$ band. As can be seen relaxation from the v'=0 vibrational state belonging to the $4p\pi$ Rydberg state to the v"=0 vibrational state in the EF curve shows a main line and the rotational components on both sides. The effect is lower in the (1;3) vibrational transition and it has disappeared when we reach the (3;9)

[1] The numbers in (0;0), (1;3), (2;6) and (3;9) are the upper and lower vibrational states of two different electronic states, according to the notation (v';v") in Herzberg [17] for example. v' meaning upper vibrational state, v" lower vibrational state of two different electronic levels.

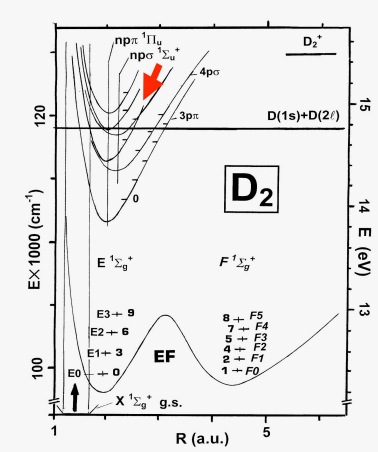

Figure 4.1: Potential curves of D_2 states studied in the present work. The $np\sigma^1\Sigma_u^+$ and $np\pi^1\Pi_u$ Rydberg states are selectively excited from the $X^1\Sigma_g^+$ ground state up to $n = 6$ using monochromatic synchrotron light and the emission to the lower $EF^1\Sigma_g^+$ is studied in a dispersed way. The potential curve of the double EF state is taken from ref. [18]. The levels of E character are $v_{EF} = 0, 3, 6, 9$ and of F character are $v_{EF} = 1, 2, 4, 5, 7, 8$. Since the E levels are closer than the F levels in internuclear distance, R, to the upper Rydberg levels, the $np\sigma, \pi - EF$ emission preferably takes place to $v_{EF} = 0, 3, 6, 9$.

vibrational transition. This can be understood looking at Fig. 4.1. The vibrational states v"=3 and v"=2 in the $4p\pi$ curve (see arrow in 4.1) are above the dissociation limit D(1s)+D(2l) so, their relaxation leads to the dissociation of the molecule with one atom in the ground state and the other one in an excited state.

Figure 4.3 shows an example of rotational analysis. With a resolution of 29 meV we are able to resolve the rotational transitions in the band. From the intensity measurements we may quantitatively determine the predissociation probability $X(R_x)$ for a given level v, J, i.e. the probability that a molecule excited to this level will predissociate. We define: $X(R_x) = 1 - \frac{R_x}{R_0}$ where R_0 is the ratio between the intensities of the P(3) line relative to that of the unresolved Q-line complex for unpredissociated levels (see Fig. 4.3) and R_x the same but for a predissociated level. Then we have,
$X(R_x = R_0) = 1 - \frac{R_0}{R_0} = 0$
$X(R_x \neq R_0) = 1 - \frac{R_x}{R_0}$
If R_0 is a fixed value and the presence of predissociation means a value $> R_0$, then, $X(R_x \neq R_0)$ increases together with the increase of predissociation. And this is what indeed happens and it is seen from the results in table 4.1.

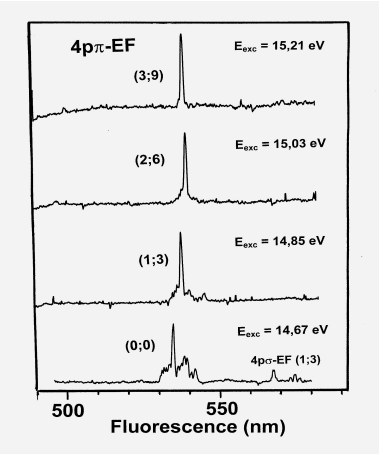

Figure 4.2: Survey scans of the 490-590 nm fluorescence region of D_2 excited by 14.67-15.21 eV photons in steps of 0.18 eV. This excitation regions corresponds to the $4p\pi - EF$ bands with $v' = 0 - 3$ and each run just shows one band (0;0),(1;3),(2;6) and (3;9) respectively. However, at the excitation with 14.67 eV photons weak traces of the $4p\sigma - EF(1;3)$ appear since the excitation energy of $4p\sigma(v = 1)$ is only 65 meV higher than that of $4p\pi(v = 0)$.

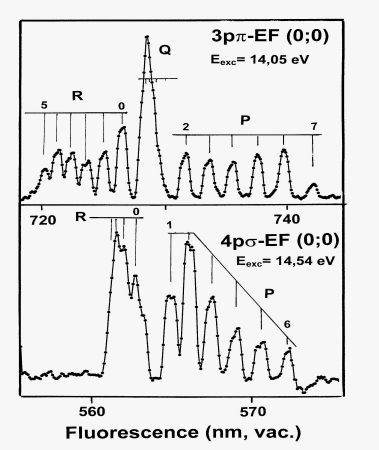

Figure 4.3: Examples of rotational analysis of $np\sigma, \pi - EF$ emission bands in D_2. The analysis has been carried out by comparisons with calculated transition energies upon known upper state [19, 20] and lower state [18] energies.

Table 4.1: Measured predissociation probabilities for denoted v-levels (J=2) of $np\pi^1\Pi^+$ Rydberg states in D_2

n	v	$X(R_x)$
3	0	0
	1	0
	2	0
	3	0
4	0	0
	1	0.32±0.20
	2	0.72±0.10
	3	0.72±0.10
5	0	0.43±0.16
	1	0.44±0.15
	2	0.24±0.20
	3	0.51±0.15
6	0	0.26±0.11
	1	0.43±0.15

Chapter 5

Water, H_2O

In this work, we have used fluorescence spectroscopy to investigate what happens to water molecules after the excitation or ionization of one of their O 1s electrons, i.e. core exciting the water molecule. Core-excited and ionized states, in general, mostly decay via the so-called Auger processes where one valence electron fills the core hole while another is ejected. In the case of core-excited neutral states below threshold, one speaks of the resonant Auger decay and distinguishes participator and spectator transitions. In a participator transition, the electron promoted to the unoccupied orbital takes part directly in the decay process, which leads to the one-hole final states that are also reached via direct valence photoionization. Spectator transitions populate final states that have two holes in the valence orbitals and an electron in an unoccupied orbital. The spectator decay is usually predominant, but the participator decay is commonly observed after core excitations to molecular orbitals. After normal and resonant Auger decays in the water molecule, most of the final states are unstable, leading to the fragmentation of the molecule. Thus, we can discuss the implications of the observed fluorescence emission for understanding the fragmentation processes of the water molecule.

5.1 Ly-α

Figure 5.1 shows the Lyman-α fluorescence yield, due to the $n = 2 \rightarrow n = 1$ transition in H, and the total ion yield measured simultaneously in the region of the O 1s excitations of water. The two curves show similar structures; hence, one can conclude that the decay of the core- excited states and subsequent dissociation yield neutral hydrogen atoms with the electron in the n = 2 shell.

But, what populates the 2p state?
One option comes from the direct dissociation of the water molecule with the hydrogen in the n=2 state. Another option comes from the cascade decay from ns, nd n≥3. After dissociation of the water molecule the H atom is left in a highly

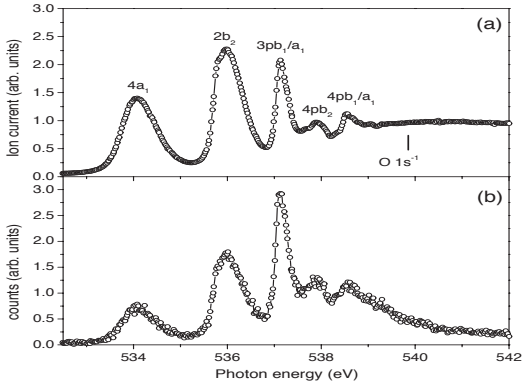

Figure 5.1: (a)The total ion yield and (b) the Lyman-α fluorescence yield measured at the O 1s edge of H_2O and normalised to the photodiode current. The most intense excitations are assigned according to [21, 22] and the O 1s ionisation threshold is marked. The two curves clearly show different intensity behaviours.

excited state, for example, 3s. This state can decay to 2p populating, therefore the 2p level.

Why $4a_1$ and $2b_2$ are depleted in the Ly-α fluorescence yield compared to the TIY?
The dissociation limit for the process $H_2O \rightarrow H(n=2) + OH^+(X^3\Sigma^-) + e^-$ is 28.31 eV. This means that the binding energies of the electron must be $\geq$ 28.31 eV. From reference [23] we learn that the Auger electrons emitted after $O1s \rightarrow 4a_1$ core excitation have mainly lower binding energies. Therefore, the population of H(n=2) in the $4a_1$ resonance is depleted compared to the the $3pb_1/a_1$ resonance. The same is true for the $2b_1$ peak. In this case the population of H(n=2) is expected to be higher than $4a_1$ and lower than $3pb_1/a_1$ [14]. There is yet another reason for the depletion of the $4a_1$ resonance. A fraction of the excitations to the antibonding molecular states, i.e., $4a_1$ decays via ultrafast dissociation [23], so the molecule breaks into H+OH before Auger decay takes place. For energy considerations the H emitted is in the ground state, therefore no Ly-α emission possible.

5.2 Neutral oxygen

Fluorescence from neutral oxygen (transition: $2p^3(^4S)3p(^3P) \rightarrow 2p^3(^4S)3s(^3S)$ was recorded across the resonances (see Fig. 5.2). The same resonances as in the total ion yield in Fig. 5.1 are clearly visible and we observe a small reduction of the $4a_1$ relative to the $2b_2$ resonance. It is more probable that neutral oxygen atoms

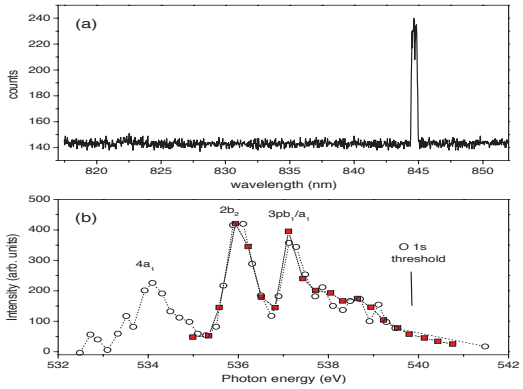

Figure 5.2: (a)The fluorescence spectrum of H_2O measured at the photon excitation energy of 535.9 eV corresponding to the $O1s \rightarrow 2b_2$ excitation. The line at 844.6 nm is due to $2p^3(^4S)3p(^3P) \rightarrow 2p^3(^4S)3s(^3S)$ transitions of neutral oxygen. The weak structure at 822.5 nm is due to $2p^3(^2D)3p(^3D) \rightarrow 2p^3(^2D)3s(^3D)$ transitions of neutral oxygen [24, 25]. (b) The intensity of the 844.6 nm oxygen line as a function of photon energy at the O 1s edge of H_2O.The curve is normalised to the photodiode current.

are mostly created in the complete dissociation of the molecular ion: $H_2O^+ \rightarrow H + O + H^+$. The dissociation limit for this reaction, referenced to the ground state of the molecule, is 23.11 eV if the two neutral atoms are in their ground states. By adding the internal energy of the oxygen atom, we find that the spectator states after the resonant Auger decay should have binding energies of at least 34.1 eV, so that this particular oxygen emission line could result. Considering the first molecular resonance ($4a_1$), for which the resonant Auger spectrum is available [23], this energy limit probably means that at least one of the final state holes should be in the inner valence orbital $2a_1$.

5.3 Neutral OH

The neutral OH fragment has an emission band around 308-320 nm due to $A^2\Sigma^+ \rightarrow X^2\Pi$ transitions. In Fig. 5.3 a series of dispersed fluorescence for the OH fragment are recorded.

Series (a) and (f) correspond to excitations below and above the threshold. In theses series, there is no presence of fluorescence, thus the fluorescence observed can be connected to the decay of neutral core-excited states. The general change in the shape of the peaks ((b)- (c)) is the result of vibrational excitations. The shift

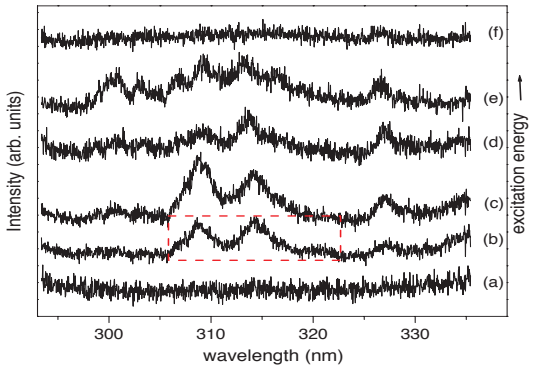

Figure 5.3: The fluorescence spectra of H_2O in the wavelength region 295-335 nm measured at the different excitation regions at the O 1s edge of water: (a) below threshold with $h\nu = 532.5 - 533.1$ eV, (b) $O1s^{-1}4a_1$resonance, (c) $O1s^{-1}2b_2$ resonance, (d) $O1s^{-1}3pb_1/a_1$ resonance, (e) $O1s^{-1}4pb_1/a_1$ resonance and (f) above threshold with $h\nu = 542.3 - 543.0$ eV. The wavelength region of the $OHA^2\Sigma^- \rightarrow X^2\Pi$ transitions is indicated by the dashed box in spectrum (b).

in the (d) and (e) series could be due to the overlapping O^+ fluorescence which occurs at neighbouring wavelengths.

5.4 OH^+

Figure 5.4 shows the fluorescence spectra in the wavelength region of the $A^3\Pi \rightarrow X^3\Sigma^-$ emission in OH^+. Again, series (a) and (f) correspond to excitations below and above the threshold, (b)-(d) correspond to the first three resonances in the TIY, respectively and (e) correspond to other Rydberg excitations. The area marked in the figure correspond to the $OH^+(A^3\Pi \rightarrow X^3\Sigma^-)$ transition at the $O1s^{-1}4a_1$ resonance. Because there is no emission at the Rydbergs series we can conclude that resonant Auger decay from core-excited Rydbergs does not populate ionic states of water which are correlated with dissociation channels yielding the $OH^+(A^3\Pi)$ ions. Thus, this emission can be explained by ultrafast dissociation followed by the resonant Auger decay of the core-excited OH fragment.

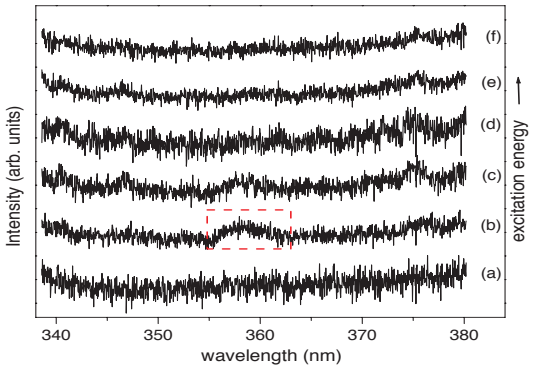

Figure 5.4: The fluorescence spectra of H_2O in the wavelength region 340-380 nm measured at the O 1 s edge of water: (a) below threshold with $h\nu = 532.5 - 533.1$eV, (b) $O1s^{-1}4a_1$ resonance, (c) $O1s^{-1}2b_2$ resonance, (d) $O1s^{-1}3pb_1/a_1$ resonance, (e) other Rydberg excitations and (f) above threshold with $h\nu = 542.3 - 543.0$ eV. The wavelength region of the $OH^+(A^3\Pi \rightarrow X^3\Sigma^-)$ emission is indicated by the dashed box in spectrum (b).

Chapter 6

Hydrogen sulphide, H_2S

In this work we have studied the visible and UV fluorescence of hydrogen sulphide after excitation with synchrotron radiation around the S 2p core level. Because of the similarity in hydrogen content and symmetry with water we expect the same trends in the fluorescence spectra.

After excitation of the S 2p electron the molecule is core-excited. Relaxation will take place via spectator Auger decay leading to a fragmentation of the molecule in a few fs. Like in water in the excitations to the antibonding molecular states ultrafast dissociation competes with the Auger decay in the time scale regime.

6.1 Total Ion Yield (TIY) and Total Fluorescence Yield (TFY)

The sulphur 2p orbital splits into the $2p_{3/2}$ and $2p_{1/2}$ levels due to spin-orbit coupling [26]. The $2p_{3/2}$ is still degenerate. This degeneracy is removed by the anisotropic molecular field. Thus, we might expect more complex spectra than for the water molecule.

Figure 6.1 shows the TFY and the TIY for H_2S. The multitude of electronic levels becomes apparent in the TIY and TFY spectra, although some visual differences can be appreciated. If we use the feature labelled A as a reference (see Fig. 6.1), one can see that the region of the antibonding orbitals (164-167 eV) is more enhanced in TFY as compared to TIY. Also its shape has been altered, showing a big resemblance to the corresponding feature seen in the partial ion yield of S^+ ions [28]. Some Rydberg excitations, particularly those labelled with D and E, appear more enhanced in TFY than in TIY. Note also that the total fluorescence intensity clearly decreases above the S 2p thresholds as compared to the core-to-Rydberg excitations, while the intensity of TIY remains high, as is expected from the production of doubly charged states by the normal Auger decay. The differences in the underlying contribution due to the core ionization makes the comparison between TFY and TIY a little difficult in the immediate threshold region, but the higher

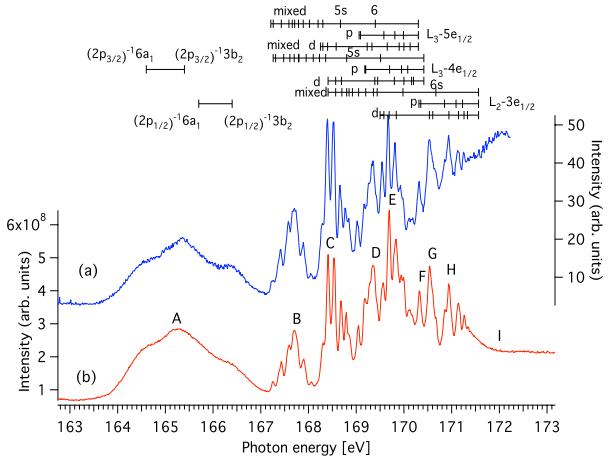

Figure 6.1: Total ion yield (a) and total fluorescence yield (b) spectra of H_2S. Assignments are after ref. [27]. Capital letters show the different energies where we measured dispersed fluorescence. Both spectra are normalised to the pressure and flux of the beamline.

Rydberg excitations such as those labelled with G and H seem to be slightly more intense in the total fluorescence. However, it is very difficult to draw any precise conclusions about fluorescence emission using only the information from the TFY .

6.2 Lyman and Balmer emission

The results of monitoring the changes in intensity of Lyman-α, Balmer-α and Balmer-β transitions by scanning the excitation energy in the range 163-173 eV are shown in Figure 6.2. The most apparent change with respect to the TIY is found in the relative intensity of the broad feature between 163-167 eV that appears clearly depressed in the Balmer-α and Lyman-α curves, compared to the intensity at the Rydberg resonances at higher energies. There are two reasons for the reduced intensity. Firstly, ultrafast dissociation of the molecule can take place at the molecular resonances. The resulting core-excited HS fragment seems to decay predominantly via spectator Auger decay [29]. The hydrogen atom, which is necessarily the other dissociation product, is concluded to be in the ground state from the dissociation limits calculated in [30], and thus cannot fluoresce. Secondly, and in the same fashion as for water an unknown fraction of the core-excited molecules will undergo resonant Auger decay before dissociation [28]. But also after the molecular resonant Auger decay, the production of excited neutral hydrogen may be proportionally more enhanced at the Rydberg resonances with respect to the molecular resonances.

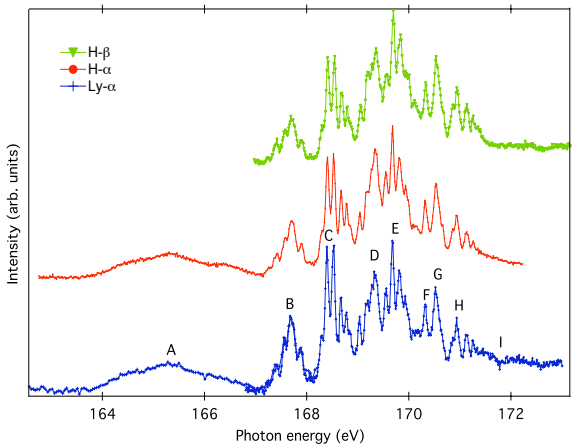

Figure 6.2: From bottom to top; Lyman-α, Balmer-α and Balmer-β emission against photon energy. Balmer-β is only shown for the Rydberg resonances. Spectra are normalised to the beamline flux and sample pressure.

At the mixed valence-Rydberg and pure Rydberg excitations, the spectator Auger decay is the predominant decay channel. In this region, the Lyman-α yield is quite similar to the total ion yield (see Fig. 6.1). In the Balmer-α and Balmer-β curves, peaks D and E are more enhanced than in TIY or even in the Lyman-α yield. In addition, the peak immediately after E as well as peak G are enhanced in the Balmer-β yield, which can be easily seen when comparing them to peak C in the Lyman-α and Balmer-α curves. Thus we observe some indications that the Balmer-β intensity tends to get proportionally more intense at higher Rydberg excitations than Balmer-α, but the trend is by far weaker than in the water molecule.

6.3 Dispersed fluorescence

Much better insight is gained from the analysis of the dispersed fluorescence data taken at different photon energies. Figure 6.3 shows an example of the dispersed fluorescence spectrum at an energy of 169.68 eV (point E in Fig. 6.1). From the dispersed fluorescence spectra we identified fluorescence coming from S^+ fragments (13 multiplets), 5 lines belonging to the Balmer series of neutral hydrogen, molecular fluorescence from HS $A\Sigma^+$-$X^2\Pi(1,0)$ and HS^+ $A^3\Pi$-$X^3\Sigma(0,0)$, and emission from neutral sulphur (4 multiplets). The results are presented in Table 6.1.

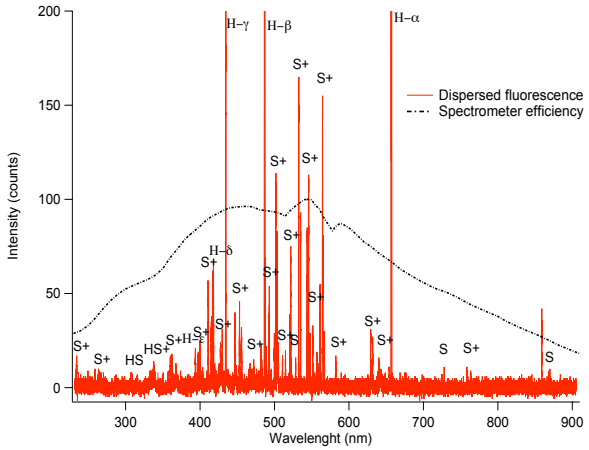

Figure 6.3: Fluorescence emission spectrum in the range of 250-900 nm from H_2S, taken at an energy of 169.68 eV. The calculated relative transmission curve of the spectrometer+CCD set-up is also shown [31].

6.4 Branching ratios

In order to follow the fluorescence of each species across the resonances we did a summation of fluorescence intensity from the different fragments detected. This summation allows us to calculate the branching rations at each of the measured energies according to the formula:

Branching ratio= $\frac{F}{W+H}$
where F is the fluorescence yield of the species and W+H is the total fluorescence yield registered.

Figure 6.4 is a plot of the calculated branching ratios and shows that the production of excited neutral hydrogen atoms is the most probable mechanism yielding fluorescence in the range 200-900 nm at the S 2p pre-edge energies. The fluorescence from neutral H atoms is the largest contribution at points B-H, with a maximum of 69% at point D, precisely at the Rydberg resonances. Moreover, the branching ratios of the Balmer-α, β and γ emissions peak at points D, E and H, respectively. They thus show the same general behaviour as observed in water. The calculated branching ratios prove the validity of the general mechanism postulated for the case of water to the case of H_2S, which by extension should be valid to any molecular system. The other major fragment contributing to the fluorescence, according to our data is S^+. This fragment is the largest contributor at point A, with 45% of the total fluorescence, and at I and and J, with branching ratios of 53% and 63%, respectively.

Table 6.1: Multiplets and their corresponding species identified in the dispersed fluorescence. Transitions are taken from NIST [24]. The wavelengths for the multiplets, bands and the H lines have been written in order to recognise lines in Fig. 6.3. For multiplets spread all over a region a dash is written and multiplets with well separated lines are written with commas.

species	transition	wavelength (nm)
S^+	$3s3p^4 - 3s^23p^2(^1D)4p$	ca 233-236
	$3s^23p^2(^1D)4p - 3s^23p^2(^1D)5d$	ca 263
	$3s^23p^2(^1D)3d - 3s^23p^2(^1D)4f$	ca 314
	$3s^23p^2(^3P)3d - 3s^23p^2(^3P)4p$	ca 359-399
	$3s^23p^2(^1D)4p - 3s^23p^2(^1D)4d$	ca 392-393,417
	$3s^23p^2(^3P)4p - 3s^23p^2(^3P)4d$	ca 402-431
	$3s^23p^2(^1D)3d - 3s^23p^2(^3P)4f$	ca 446-448
	$3s^23p^2(^1D)4s - 3s^23p^2(^1D)4p$	ca 452-455
	$3s^23p^2(^3P)4s - 3s^23p^2(^3P)4p$	ca 456-521
	$3s^23p^2(^1D)3d - 3s^23p^2(^3P)5p$	ca 495,507
	$3s^23p^2(^1D)4p - 3s^23p^2(^3P)4d$	532
	$3s^23p^2(^3P)3d - 3s^23p^2(^3P)4p$	ca 627-641
	$3s^23p^2(^1D)3d - 3s^23p^2(^1D)4p$	757,762
HS	$A\Sigma^+ - X^2\Pi(1,0)$	306
HS^+	$A^3\Pi - X^3\Sigma(0,0)$	336
H	$2-7$	397
	$2-6$	410
	$2-5$	434
	$2-4$	486
	$2-3$	656
S	$3s^23p^3(^4S^*)4s - 3s^23p^3(^4S^*)5p$	527
	$3s^23p^3(^4S^*)4p - 3s^23p^3(^4S^*)6d$	653
	$3s^23p^3(^4S^*)4p - 3s^23p^3(^4S^*)5d$	724
	$3s^23p^3(^4S^*)4p - 3s^23p^3(^4S^*)4d$	ca 867-869

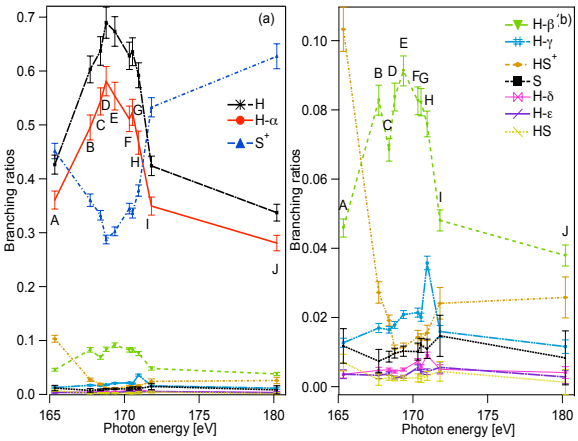

Figure 6.4: Branching ratios of the different fragments against photon energy. From top to the bottom at 180 eV (point J) the traces are: S^+,H and $H-\alpha$ in (a). (b) is an inset of (a) for the low intensity traces and they correspond from top to bottom to: $H-\beta$, HS^+, $H-\gamma$, S, $H-\delta$, $H-\epsilon$ and HS.

6.5 Dissociation pathways

We also analysed the different dissociation pathways taking place in the H_2S molecule across the resonances. At point A in Fig. 6.1, for example, there are two different mechanisms at play. On the one hand, ultrafast dissociation competes with Auger decay, and the result is that the core-excited molecule breaks apart into core-excited HS namely, HS^{**} and a hydrogen atom in the ground state. The core excited HS molecule will mostly undergo spectator Auger decay [29] and the result will generally be an excited configuration of the HS^+ molecular ion that can further dissociate to yield S^+ and H (see below).

$$
\begin{aligned}
H_2S + h\nu &\rightarrow HS^{**} + H \\
HS^{**} &\rightarrow HS^{+*} + e^- \\
HS^{+*} &\rightarrow H^* + S^+ \quad or \quad H + S^{+*}
\end{aligned}
$$

On the other hand, the core-excited H_2S molecule can decay before it dissociates, and this process takes place also at energies below the ionisation thresholds (see set of equations below). Then the final state is either a valence-single-hole configuration of H_2S^+, due to participator Auger decay, which has been argued as not negligible in [28] despite the reasonings in [29], or a much more energetic valence-two-holes configuration of the molecular parent ion reached after spectator Auger decay. Neutral hydrogen atoms and S^+ ions would then be produced from the dissociation of the different final Auger states of the molecular parent ion.

$$
\begin{gathered}
H_2S + h\nu \rightarrow H_2S^{**} \\
H_2S^{**} \rightarrow H_2S^{+*} + e^- \\
H_2S^{+*} \rightarrow H^* + HS^+ \quad or \quad H + HS^{+*} \\
HS^{+*} \rightarrow H^* + S^+ \quad or \quad H + S^{+*}
\end{gathered}
$$

Chapter 7

Pyrimidine, $C_4H_4N_2$

Here I want to present the preliminary results we have got after applying PIFS technique to pyrimidine.

Pyrimidine (see Fig. 7.1) together with purine are the precursors which form the well known structure of the life code, DNA.

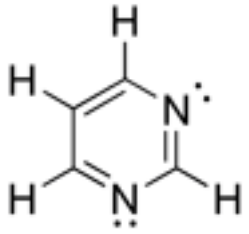

Figure 7.1: Pyrimidine molecule taken from [8].

The electronic ground state configuration of pyrimidine in the C_{2v} symmetry group is: $(1a_1)^2(1b_2)^2(2a_1)^2(2b_2)^2(3a_1)^2(4a_1)^2(3b_2)^2(5a_1)^2(4b_2)^2(6a_1)^2(1b_1)^2(7a_1)^2$ $(1a_2)^2(5b_2)^2(2b_1)^2(8a_1)^2(9a_1)^2(6b_2)^2(10a_1)^2(11a_1)^2(7b_2)^2$ which makes a total of 42 electrons. The core levels and inner valence orbitals are $(1a_1)^2(1b_2)^2(2a_1)^2(2b_2)^2$ $(3a_1)^2(4a_1)^2$ [32] and the rest (form $3b_2$ to $7b_2$ are the outer valence molecular orbitals. Figure 7.2 shows three different fluorescence yields for pyrimidine at both C 1s and N 1s edges and the TIY after C 1s and N 1s excitations. The TIY shows the transitions from the core level C 1s (a_1 symmetry) to unoccupied molecular and Rydberg states, like $2a_1, 8b_2, 3b_1$ or $2a_2$ for example. Our TIY spectra in both edges resolve at least the same features shown in ref. [33] though no assignment of the peaks is done in the paper. As can be seen in Fig. 7.1 pyrimidine is a low-symmetry molecule. It has 3 different environmental carbons meaning 3 different thresholds situated between 290 and 293 eV [33]. The overlap of electronic

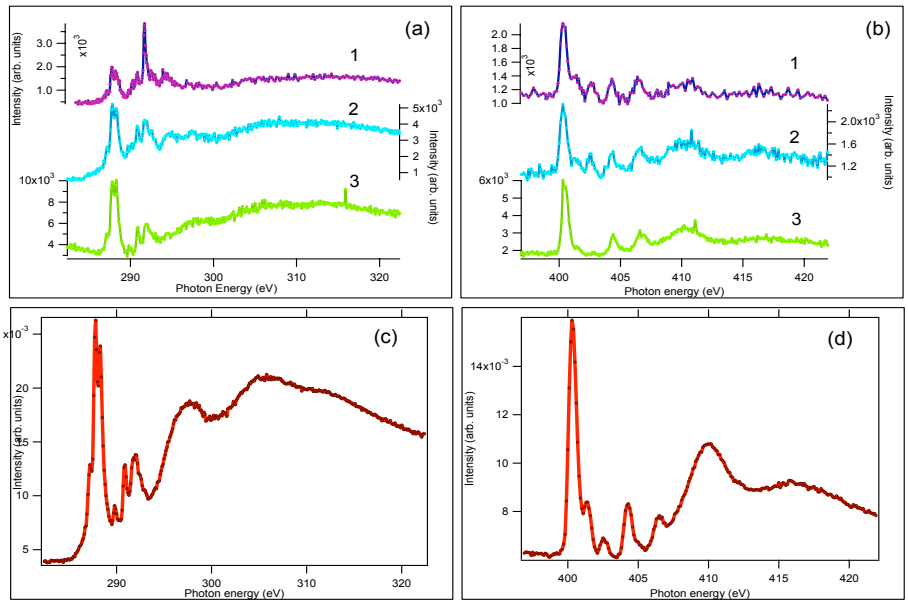

Figure 7.2: (a) and (c) are the respective fluorescence and ion yield at the C 1s edge. (b) and (d) are the same but at the N 1s edge. Number 1 in the top graphs is the Ly-α (123 nm) fluorescence yield. Number 2 is the fluorescence yield in the 200-300 nm and number 3 is the fluorescence recorded for the 300-600 nm range.

transitions converging to these thresholds and the possible vibrational fine structure makes an assignment difficult without a theoretical calculation. As a general result, peaks below 293 eV in the C edge (see Fig. 7.2) correspond to transitions to unoccupied molecular and Rydberg states of the molecule. The big bumps of higher energy could correspond to shape resonances, i.e., transitions to a $\sigma*$ orbital. The N edge for pyrimidine is at 405 eV and if we consider valid the latter argument, we could interpret the pyrimidine N 1s spectra as a series of electronic transitions to the unoccupied molecular and Rydberg orbitals below the threshold. Above threshold, transitions to the unoccupied $\sigma*$ orbitals would be responsible for the broad features.

The preliminary results for the fluorescence are also shown. The general tendency seen in small hydride molecules where the Ly-α spectrum is similar to the TIY [13, 10] seems not to hold here and instead the TFY in the visible range shows a higher resemblance to the TIY. A detailed study of dispersed fluorescence would allow us to detect the fragments fluorescing and to interpret the fluorescence.

Our first approach has been for pyrimidine. Next step is to study its oxidised form which lead to the study of DNA pyrimidinic bases, cytosine and thymine. We are also interested in the pyrimidine analogues (pyridazine and pyrazine) because,

more generally, we want to deepen our knowledge of nitrogen double substitutes heteroaromatic systems which constitute the basis of more complex biomolecules.

Part III

What is next?

Chapter 8

Outlook

I can think of two kind of approaches for future experiments. The real one and the one which is beyond my PhD for time reasons.

The feasible or real one includes absolute cross-sections measurements of small biomolecules. To begin with it would be interesting to measure the aza-bencenes family; pyridine, pyrimidine (DNA precursor), pyrazine, pyridazine and s-triazine. Continuing then with the study of purine, the other DNA precursor. If the results are satisfactory we could think of studying the four DNA bases, Thymine (T), Guanine (G), Citosine (C) and Adenine (A) as well as Uracil (U) which is the base for RNA. To our knowledge no fluorescence studies with SR in the Vis-UV range after core-excitations are done for these molecules, thus it can lead to a new field of results. Some of these molecules are solid at normal conditions, therefore, in order to perform such experiments some modifications to our experimental set up need to be done. In the same line of investigations and if our project receive beamtime, I would like to continue studying the the building blocks of proteins, so called, amino acids. This would contribute to the necessary knowledge for a jump into the condensed phase later on and study the real cell damage.

The one that is beyond the scope of my PhD, because of time reasons would be, as I mentioned, to jump into the condensed phase and study the secondary effects created after the interaction of high energy photons with biological systems. As is well known, when high energy photons interact with biological systems they create large amounts of low energy secondary electrons and ions, which do subsequent damage to, e.g., the cell's DNA. So the goal would be to study the interaction of the same molecules with low-energy electrons.

Bibliography

[1] D. Attwood, *Soft X-rays and extreme ultraviolet radiation* Cambridge University Press (2000) USA

[2] *Max-lab activity report 2004*

[3] Max-lab official web site: *www.maxlab.lu.se*

[4] M. Bässler, A. Ausmees, M. Jurvansuu, R. Feifel, J.-O.Forsell, P. de Tarso Fonseca, A. Kivimäki, S. Sundin, S. L. Sorensen, R. Nyholm, O. Björneholm, S. Aksela and S. Svensson, *Nucl. Instr. Methods in Phys. Research* **A469** (2001) 382

[5] K.C. Prince, R. R. Blyth, R. Delaunay, M. Zitnik, J. Krempasky, J. Slezak, R. Camilloni, L. Avaldi, M. Coreno, G. Stefani, C. Furlani, M. de Simone and S. Stranges *J. Synchrotron Radiat.* **5** (1989) 565

[6] ELETTRA official web site: *www.elettra.trieste.it*

[7] Hyperphyiscs web site: *http://hyperphysics.phyastr.gsu.edu/hbase/hframe.html*

[8] Wikipedia web site: *http://en.wikipedia.org/wiki/Main_Page*

[9] G. Vall-llosera, Master's Degree Project: *Absolute Intensity Calibration of a Visible- UV Spectrometer and Application to Dispersed Fluorescence Measurements* TRITA-FYS 2004:58 ISSN 0280-316X (2004)

[10] G. Vall-llosera, E. Melero García, A. Kivimäki, E. Rachlew, M. Coreno, M. de Simone, R. Richter and K.C. Prince *submitted to PCCP* (2006)

[11] G. Vall-llosera, J. Álvarez Ruiz, P. Erman, E. Melero García, E. Rachlew, S. Menmuir and M. Stankiewicz *J. Phys. B: At. Mol. Opt. Phys.* **38** (2005) 659

[12] J. Álvarez Ruiz, E. Melero García, A. Kivimäki, M. Coreno, P. Erman, E. Rachlew and R. Richter *J. Phys. B: At. Mol. Opt. Phys.* **38** (2005) 387

[13] A. Kivimäki, M. Coreno, R. Richter, J. Álvarez Ruiz, E. Melero García, M. de Simone, V. Feyer, G. Vall-llosera and K. C. Prince. *J. Phys. B: At. Mol. Opt. Phys.* **39** (2006) 1101

[14] E. Melero García, A. Kivimäki, L.G.M. Pettersson, J. Álvarez Ruiz, M. Coreno, M. de Simone, R. Richter and K. C. Prince *Phys. Rev. Lett.* **96** (2006) 063003

[15] M. Stankiewicz , E. Melero García, J. Álvarez Ruiz, P. Erman, P. A. Hatherly, A. Kivimäki, E. Rachlew and J. Rius i Riu *Rev. Sci. Inst.* **75** (2004) 2402

[16] U. Fantz and D Wünderlich *IAEA Int. Nucl. Data Committee IND(NDS)* **457** (2004)

[17] F.R.S., Gerhard Herzberg, *Molecular spectra and molecular structure; I. spectra of diatomic molecules* Krieger publishing company (1950) USA

[18] S. Yu and K. Dressler *J. Chem. Phys.* **101** (1994) 7692

[19] P. Senn, O. Quadrelli, K. Dressler and G. Herzberg *J.Chem. Phys.* **85** (1986) 2384

[20] A. Monfils *J. Mol. Spectrosc.* **15** (1965) 265

[21] J. Schirmer, A. B. Trofimov, K. J. Randall, J. Feldhaus, A. M. Bradshaw, Y. Ma, C. T. Chen and F. Sette *Phys. Rev. A* **47** (1993) 1136

[22] K. Okada, K. Ueda, T. Tokushima, Y. Senba, H. Yoshida, Y. Shimizu, M. Simon, H. Chiba, H. Okumura, Y. Tamenori et al. *Chem. Phys. Lett.* **326** (2000) 314

[23] I. Hjelte, M. N. Piancastelli, R. F. Fink, O. Björneholm, M. Bässler, R. Feifel, A. Giertz, H. Wang, K. Wiesner, A. Ausmees et al. *Chem. Phys. Lett.* **334** (2001) 151

[24] NIST web site: *http://physics.nist.gov/PhysRefData/ASD/index.html*

[25] A. Karawajczyk, P. Erman, E. Rachlew-Kälne, J. Rius i Riu, M. Stankiewicz, K. Yoshiki Franzén and L. Veseth *Phys. Rev.* **A61** (2000) 032718

[26] S. Svensson, A. Ausmees, S. J. Osborne, G. Bray, F. Gel'mukhanov, H. Ågren, A. Naves de Brito, O.-P. Sairanen, A. Kivimäki, E. Nõmmiste, H. Aksela and S. Aksela *Phys. Rev. Lett.* **72** (1994) 3021

[27] E. Hudson, D. A. Shirley, M. Domke, G. Remmers and G. Kaindl *Phys. Rev.* **A49** (1994) 161

[28] R. Guillemin, W. C. Stolte, L. T. N. Dang, S-W. Yu and D. W. Lindle *J. Chem. Phys.* **122** (2005) 094318

[29] H. Aksela , S. Aksela , A. Naves de Brito, G. M. Bancroft and K. H. Tan *Phys. Rev.* **A45** (1992) 7948

[30] A. Naves de Brito and H. Ågren *Phys. Rev.* **A45** (1992) 7953

[31] M. Coreno , K. C. Prince , R. Richter , M. de Simone , K. Bucar and M. Žitnik *Phys.Rev.* **A72** (2005) 052512

[32] A. W. Potts, D. M. P. Holland, A. B. Trofimov, J. Schirmer, L. Karlsson and K. Siegbahn *J. Phys. B: At. Mol. Phys.* **36** (2003) 3129

[33] O. Plashkevych, A. Snis, L. Yang, H. Ågren and S. F. Matar *Physica Scripta* **63** (2001) 70